Conversion efficiency in the process of copolarized spontaneous four-wave mixing

Karina Garay-Palmett,[1,2] Alfred B. U'Ren,[1] and Raúl Rangel-Rojo[2]

[1]*Instituto de Ciencias Nucleares, Universidad Nacional Autónoma de México, Apartado Postal 70-543, 04510 DF, México*

[2]*Departamento de Óptica, Centro de Investigación Científica y de Educación Superior de Ensenada, Apartado Postal 2732, Ensenada, BC 22860, México*

(Received 24 May 2010; published 8 October 2010)

We study the process of copolarized spontaneous four-wave mixing in single-mode optical fibers, with an emphasis on an analysis of the conversion efficiency. We consider both the monochromatic-pump and pulsed-pump regimes, as well as both the degenerate-pump and nondegenerate-pump configurations. We present analytical expressions for the conversion efficiency, which are given in terms of double integrals. In the case of pulsed pumps we take these expressions to closed analytical form with the help of certain approximations. We present results of numerical simulations, and compare them to values obtained from our analytical expressions, for the conversion efficiency as a function of several key experimental parameters.

DOI: 10.1103/PhysRevA.82.043809 PACS number(s): 42.50.Dv, 03.65.Ud, 42.65.Hw

I. INTRODUCTION

Photon-pair sources based on spontaneous parametric processes have represented a crucial enabling technology for fundamental tests of quantum mechanics [1] and for the implementation of quantum-information processing protocols [2]. An important distinction among spontaneous parametric photon-pair sources is whether they are based on second-order nonlinearities in crystals [3], or on third-order nonlinearities, often in optical fibers [4,5]. In the first case, we refer to the process as spontaneous parametric down-conversion (SPDC), while in the second case we refer to the process as spontaneous four-wave mixing (SFWM). The fact that two pump photons are annihilated per photon-pair generation event in the case of SFWM rather than only one, as in the case of SPDC, represents the key underlying difference between these two processes. This essential difference can make SFWM sources superior in terms of a greater ability to engineer the photon-pair properties [6], and in terms of a different dependence of the emitted flux on certain experimental parameters, which favors bright photon-pair sources.

Of course, an important consideration in the design and implementation of photon-pair sources is the emission flux, or equivalently, the conversion efficiency. On the one hand, the ability to compare the expected flux in a number of different experimental situations is an important tool for the design of specific sources and experiments. On the other hand, our understanding of a photon-pair source is not complete without a full appreciation of the dependence of the conversion efficiency on all relevant experimental parameters. The motivation behind this paper is to present specific analytic expressions for the conversion efficiency expected in the spontaneous four-wave mixing process in optical fibers. While we restrict our attention to copolarized SFWM (i.e., we assume the same polarization for all four fields) and likewise we restrict our treatment to cases where all four fields propagate in the fundamental fiber mode, we consider a number of other source variations. Specifically, we consider both pulsed and monochromatic pumps, as well as both degenerate and nondegenerate pumps. We derive expressions for the conversion efficiency in the form of integrals, which where possible we take to closed analytic form under certain approximations. We compare values derived from numerical integration of the conversion efficiency expressions (without resorting to approximations) to corresponding values derived from expressions in closed analytic form. We also note that this work could be extended in a straightforward manner to also incorporate the cases of cross-polarized SFWM, and of the SFWM process in birefringent fibers.

Let us note that for second-order nonlinear processes which are stimulated in nature, such as second-harmonic generation, the emitted flux scales as the square of the incident pump power, and scales linearly with the pump bandwidth [7]. This is a result of the fact that two pump photons are combined to generate each second-harmonic photon. In the case of SFWM, even though the process is spontaneous in nature, two pump photons are likewise involved in every photon-pair generation event. This leads to the same dependence of emitted flux on pump power and pump bandwidth, for spontaneous four-wave mixing in a third-order nonlinear medium, as compared to (stimulated) second-harmonic generation in a second-order nonlinear medium. This is to be contrasted with SPDC for which the emitted flux scales linearly with pump power and is constant (within the phase-matching bandwidth) with respect to the pump bandwidth. The fact that in some respects SFWM sources behave essentially as a stimulated process would in a second-order nonlinear medium, coupled with the long interaction lengths possible, favors SFWM over SPDC sources in terms of the attainable photon-pair flux. As a concrete illustration, in a remarkable recent SPDC experiment [8], despite extensive source optimization, the observed photon-pair flux is $\sim$500 times lower than that in a representative SFWM experiment [9], when computing the flux per unit pump power and per unit emission bandwidth.

While some previous works have analyzed the emitted flux in the SFWM process [10–12], in this paper we aim to present a unified approach leading to explicit conversion efficiency expressions, together with corresponding numerical simulations, valid for the pulsed- and monochromatic-pump regimes, as well as for the degenerate- and nondegenerate-pump configurations.

II. DERIVATION OF THE RATE OF EMISSION

In this paper we study the process of spontaneous four-wave mixing in optical fibers, in which nonlinear phenomena originate from the third-order susceptibility $\chi^{(3)}$. In this process, two photons (one from each of two pump fields E_1 and E_2) can be jointly annihilated to give rise to the emission of a photon pair comprised of one photon in the signal mode $\hat{E}_s$ and one photon in the idler mode $\hat{E}_i$. In our analysis we assume that all fields propagate in the same direction along the fiber (which defines the z axis), and in the fundamental transverse mode supported by the fiber. The electric fields can be written in the form $E_\mu = (E_\mu^{(+)} + E_\mu^{(-)})/2$; the superscripts $(+)$ and $(-)$ denote the positive- and negative-frequency parts of the electric field. While we assume that all four participating fields are linearly polarized, parallel to the x axis, our analysis could be adapted to cross-polarized spontaneous four-wave mixing processes. In this paper, we specifically focus on the rate of emission of photon-pair sources based on spontaneous four-wave mixing in optical fiber.

It can be shown that the SFWM process is governed by the following Hamiltonian:

$$\hat{H}(t) = \frac{3}{4}\epsilon_o \chi^{(3)} \int d^3\mathbf{r} E_1^{(+)}(\mathbf{r},t) E_2^{(+)}(\mathbf{r},t) \times \hat{E}_s^{(-)}(\mathbf{r},t)\hat{E}_i^{(-)}(\mathbf{r},t), \quad (1)$$

where the integration is carried out over the portion of the nonlinear medium which is illuminated by the pump fields, and ϵ_o is the vacuum electrical permittivity.

The quantized signal and idler fields can be written in the form

$$\hat{E}^{(+)}(\mathbf{r},t) = i\sqrt{\delta k} f(x,y) \sum_k \exp[-i(\omega t - kz)]\ell(\omega)\hat{a}(k), \quad (2)$$

where the angular frequency ω is a function of k, as defined by the dispersion relation. $\delta k = 2\pi/L_Q$ is the mode spacing, written in terms of the quantization length L_Q. Function $\ell(\omega)$ is given as

$$\ell(\omega) = \sqrt{\frac{\hbar\omega}{\pi\epsilon_o n^2(\omega)}}, \quad (3)$$

in terms of the (linear) refractive index of the nonlinear medium $n(\omega)$ and of Planck's constant $\hbar$. In Eq. (2), $\hat{a}(k)$ is the annihilation operator associated with the fundamental propagation mode in the fiber, and $f(x,y)$ represents the transverse spatial distribution of the field, which is normalized so that $\int\int |f(x,y)|^2 dxdy = 1$, and which is here approximated to be frequency-independent within the bandwidth of the signal and idler modes.

In our analysis, we assume that the two pumps can be well described by classical fields, expressed in terms of their Fourier components as

$$E_\nu^{(+)}(\mathbf{r},t) = A_\nu f_\nu(x,y) \int d\omega \alpha_\nu(\omega) \exp\{-i[\omega t - k(\omega)z]\}, \quad (4)$$

where, for each of the two pump fields ($\nu = 1,2$), A_ν is the amplitude, $\alpha_\nu(\omega)$ is the spectral envelope with normalization $\int d\omega |\alpha_\nu(\omega)|^2 = 1$, and $f_\nu(x,y)$ is the transverse spatial distribution. Functions $f_\nu(x,y)$ are approximated to be frequency-independent within the spectral width of the pump pulses and exhibit the same normalization as their signal and idler counterparts [see Eq. (2)]. It can be shown that A_ν is related to pump peak power, P_ν, according to the relation

$$A_\nu = \left[\frac{2P_\nu}{\epsilon_o c n_\nu \left|\int d\omega \alpha_\nu(\omega)\right|^2}\right]^{1/2}, \quad (5)$$

in terms of $n_\nu \equiv n(\omega_\nu^o)$, where ω_ν^o represents the carrier frequency for pump ν.

By replacing Eqs. (2) and (4) into Eq. (1), and following a standard perturbative approach [13], it can be shown that the two-photon state produced by spontaneous four-wave mixing is given by $|\Psi\rangle = |0\rangle_s|0\rangle_i + \zeta|\Psi_2\rangle$, where $|\Psi_2\rangle$ is the two-photon component of the state

$$|\Psi_2\rangle = \sum_{k_s}\sum_{k_i} G_k(k_s,k_i)\hat{a}^\dagger(k_s)\hat{a}^\dagger(k_i)|0\rangle_s|0\rangle_i, \quad (6)$$

written in terms of the joint amplitude $G_k(k_s,k_i)$ and a constant ζ, related to the conversion efficiency

$$\zeta = i\frac{3(2\pi)\chi^{(3)}\epsilon_o L\delta k}{4\hbar} A_1 A_2 \int dx \int dy f_1(x,y) \times f_2(x,y) f_s^*(x,y) f_i^*(x,y). \quad (7)$$

The function $G(\omega_s,\omega_i) = \ell(\omega_s)\ell(\omega_i)F(\omega_s,\omega_i)$ results from writing $G_k(k_s,k_i)$ in terms of frequencies rather than wave numbers and represents the joint spectral amplitude, written in terms of the function $F(\omega_s,\omega_i)$ given by

$$F(\omega_s,\omega_i) = \int d\omega \alpha_1(\omega)\alpha_2(\omega_s+\omega_i-\omega) \times \mathrm{sinc}\left[\frac{L}{2}\Delta k(\omega,\omega_s,\omega_i)\right] e^{i\frac{L}{2}\Delta k(\omega,\omega_s,\omega_i)}. \quad (8)$$

Note that the spectral dependence of $\ell(\omega)$ [see Eq. (3)] tends to be slow over the frequency range of interest. If this dependence is neglected [14], the photon-pair spectral properties are fully determined by function $F(\omega_s,\omega_i)$, which from this point onward we refer to as the joint spectral amplitude function. In Eq. (8), $\Delta k(\omega,\omega_s,\omega_i)$ represents the phase mismatch, given by

$$\Delta k(\omega,\omega_s,\omega_i) = k(\omega) + k(\omega_s+\omega_i-\omega) - k(\omega_s) - k(\omega_i) - (\gamma_1 P_1 + \gamma_2 P_2), \quad (9)$$

which includes a nonlinear contribution $(\gamma_1 P_1 + \gamma_2 P_2)$ derived from self-phase and cross-phase modulation, where γ_ν is the nonlinear coefficient given by

$$\gamma_\nu = \frac{3\chi^{(3)}\omega_\nu^o}{4\epsilon_o c^2 n_\nu^2 A_{\mathrm{eff}}^\nu}. \quad (10)$$

In the above expression, we have defined $n_\nu \equiv n(\omega_\nu^o)$ and the effective area $A_{\mathrm{eff}}^\nu \equiv [\int\int dxdy |f_\nu(x,y)|^4]^{-1}$, in terms of the carrier frequency ω_ν^o for pump mode ν [15,16].

For ease of calculating the emitted flux for fiber-based SWFM sources, we assume that the photon pairs, once generated in the fiber of length L considered in our calculation, propagate along a continuation of this fiber to the detectors,

in such a way that no further photon pairs are produced. In a realistic experiment this could be achieved by suppressing pump photons through the use of appropriate spectral filters. Thus, the (linear) optical properties of the fiber through which the photon pairs propagate in order to reach the detectors are assumed to be identical to those of the fiber length where generation takes place. Likewise, we assume that the photon pairs are split into separate spatial signal and idler modes (e.g., with a fiber-based beam splitter), and we refer to the count rate of an individual mode (e.g., the signal mode) as the source brightness. In order to proceed with our analysis, we are interested in the expectation value of the signal-mode energy density given by

$$u(\mathbf{r},t) = \tfrac{1}{2}\langle\Psi_2|\hat{E}_s^{(-)}(\mathbf{r},t)\hat{D}_s^{(+)}(\mathbf{r},t)|\Psi_2\rangle, \tag{11}$$

where $\hat{D}_s(\mathbf{r},t) = \epsilon\hat{E}_s(\mathbf{r},t)$ is the signal-mode electric displacement operator, ϵ is the medium permittivity, and $\hat{E}_s$ is given according to Eq. (2). Nevertheless, since propagation occurs along the z axis, it is convenient to calculate the linear energy density $u_z(z,t)$ by integrating $u(\mathbf{r},t)$ over the transverse coordinates x and y. Consequently, replacing Eqs. (2) and (6) into Eq. (11), we can show that

$$u_z(z,t) = \vartheta\int dk_s\int dk_s'\int dk_i\,\ell[\omega(k_s)]\ell_D[\omega(k_s')]G^*(k_s,k_i) \times G(k_s',k_i)e^{-i[\omega(k_s')-\omega(k_s)]t}e^{-i(k_s-k_s')z}, \tag{12}$$

where $\vartheta = 2|\zeta|^2/(\delta k)^2$ (note that ζ is linear in δk so that ϑ is constant with respect to δk) and is explicitly given by

$$\vartheta = \frac{2^3(2\pi)^2\epsilon_o^2 n_1 n_2 c^2}{\hbar^2\omega_1^o\omega_2^o}\frac{L^2\gamma^2P_1P_2}{\left|\int d\omega\alpha_1(\omega)\right|^2\left|\int d\omega\alpha_2(\omega)\right|^2}, \tag{13}$$

and $\ell_D(\omega) = \epsilon_o n^2\ell(\omega)$. The linear energy density, see Eq. (12), has been written in terms of the nonlinear coefficient γ [17] [which is different from γ_1 and γ_2 of Eq. (10)], defined as

$$\gamma = \frac{3\chi^{(3)}\sqrt{\omega_1^o\omega_2^o}}{4\epsilon_o c^2 n_1 n_2 A_{\text{eff}}}, \tag{14}$$

where A_{eff} is the effective interaction area among the four fields given by

$$A_{\text{eff}} = \frac{1}{\int dx\int dy f_1(x,y)f_2(x,y)f_s^*(x,y)f_i^*(x,y)}. \tag{15}$$

Note that the above expression for A_{eff} takes into account the normalization assumed for the transverse spatial distribution of each of the four modes which participate in the process of SFWM.

In Eq. (12), k-vector sums have been converted to integrals, which can be done in the limit $L_Q\to\infty$, so that $\delta k\sum_k\to\int dk$. This equation gives the signal-mode linear energy density. The total signal-mode energy can be obtained by integrating $u_z(z,t_0)$, evaluated at a given time t_0, over coordinate z within the spatial extent of the generated biphoton wave packets. For this calculation, we consider two cases: (i) pulsed-pump fields and (ii) monochromatic-pump fields, which are addressed in the following two subsections.

A. Pulsed-pump regimes

In order to carry out further calculations for the specific case of pulsed pumps, we limit our treatment to pump fields with a Gaussian spectral envelope, which can be written in the form

$$\alpha_\nu(\omega) = \frac{2^{1/4}}{\pi^{1/4}\sqrt{\sigma_\nu}}\exp\left[-\frac{(\omega-\omega_\nu^o)^2}{\sigma_\nu^2}\right], \tag{16}$$

where ω_ν^o represents the central frequency and σ_ν defines the bandwidth. Replacing Eqs. (3), (8), (13), and (16) into Eq. (12), we obtain the following expression for the SFWM signal-mode energy produced by an isolated mode-1 pump pulse interacting with an isolated mode-2 pump pulse:

$$U_s = \int_{-\infty}^{\infty}dz u_z(z,t_0) = \frac{2^6\hbar c^2 n_1 n_2}{\pi^2\omega_1^o\omega_2^o}\frac{L^2\gamma^2P_1P_2}{\sigma_1^2\sigma_2^2} \times\int d\omega_s\int d\omega_i\frac{\omega_s^2k^{(1)}(\omega_s)}{n^2(\omega_s)}\frac{\omega_i k^{(1)}(\omega_i)}{n^2(\omega_i)}|f(\omega_s,\omega_i)|^2, \tag{17}$$

in terms of a version of the joint spectral amplitude [see Eq. (8)] defined as $f(\omega_s,\omega_i) = (\pi\sigma_1\sigma_2/2)^{1/2}F(\omega_s,\omega_i)$, which does not contain factors in front of the exponential and sinc functions so that all factors appear explicitly in Eq. (17). Note that the signal-mode energy density has appreciable values within the overlap region between the two pump pulses along z; because we are considering for this calculation a single isolated pulse for each of the two pump modes, we have extended the integration limits to $\pm\infty$ in Eq. (17). In the derivation of this equation, integrals over k_s and k_i were transformed to frequency integrals through the relation $dk = k^{(1)}(\omega)d\omega$, where $k^{(1)}(\omega)$ represents the first frequency derivative of $k(\omega)$.

In order to calculate the number of signal-mode photons generated per mode-1 and mode-2 pump pulse pair, we first express U_s in terms of the signal-mode spectral energy density, $u_s(\omega_s)$, defined such that $U_s = \int d\omega_s u_s(\omega_s)$. The corresponding spectral photon number density is then given by $\mathcal{N}_s(\omega_s) = u_s(\omega_s)/(\hbar\omega_s)$ and finally the total emitted-photon number is obtained as $N_s = \int d\omega_s\mathcal{N}_s(\omega_s)$.

We are interested in calculating the conversion efficiency in the copolarized SFWM process, which we define as $\eta = N_s/N_p$, where $N_p = N_1 + N_2$; here, N_ν is the number of photons per pump pulse for each of two pump modes (with $\nu = 1,2$). For sufficiently narrow-band pump pulses, it is acceptable to write $N_\nu = U_\nu/(\hbar\omega_\nu^o)$, where U_ν is the energy per pulse in mode ν. In this case, we arrive at the following expression for N_ν:

$$N_\nu = \frac{\sqrt{2\pi}P_\nu}{\hbar\omega_\nu^o\sigma_\nu}. \tag{18}$$

The photon-pair conversion efficiency can then be written as

$$\eta = \frac{2^8\hbar^2c^2n_1n_2}{(2\pi)^3}\frac{L^2\gamma^2N_1N_2}{\sigma_1\sigma_2(N_1+N_2)} \times\int d\omega_s\int d\omega_i\frac{\omega_s k_s^{(1)}}{n_s^2}\frac{\omega_i k_i^{(1)}}{n_i^2}|f(\omega_s,\omega_i)|^2. \tag{19}$$

Through Eq. (19), we may gain an understanding of the dependence of the conversion efficiency on various experimental

parameters, including the fiber length L, the pump peak powers (P_1 and P_2) and the pump bandwidths (σ_1 and σ_2). Besides these parameters, the conversion efficiency of course also exhibits a dependence on fiber dispersion properties through the phase mismatch [see Eq. (9)]. From Eq. (19), it is clear that η varies quadratically with the nonlinear coefficient γ, which implies that it has an inverse fourth power dependence on the transverse mode radius [15]. This means that, in general, a small core radius leads to large rates of emission (note that this trend may be reverted for sufficiently narrow fibers for which the mode radius can increase as the core radius is reduced [18,19]).

The dependence on pump peak power is clear from Eq. (19), where N_ν is linear in P_ν according to Eq. (18). As expected, N_s exhibits a quadratic dependence on the pump power (or, alternatively, η exhibits a linear dependence on the pump power), which is more evident for degenerate pumps, for which $P_1 = P_2 \equiv P$. This behavior represents an important difference with respect to photon-pair sources based on SPDC in second-order nonlinear crystals, for which N_s is linear in pump power. In fact, a quadratic dependence of the generated power on the pump power, in the case of second-order nonlinear optics, is associated with stimulated processes such as second-harmonic generation rather than with spontaneous processes. This quadratic pump-power scaling represents a clear advantage of the process of SFWM over SPDC, in terms of the attainable photon-pair flux, for the design of bright photon-pair sources. Note that because the phase mismatch has an additive term which is linear in P_1 and P_2, for large enough pump powers there can be a deviation from this stated quadratic dependence.

In common with SPDC, a concern with SFWM is that for sufficiently high conversion efficiencies, multiple photon pairs can be generated at a given time. This represents a limitation, since many experiments rely on the emission of individual photon pairs, i.e., which can be well isolated from other photons both spatially and temporally. Thus, for example, the existence of multiple-pair amplitudes implies that a detection event (with a nonphoton-number resolving detector), say in the idler mode of an SPDC source, cannot herald a true single photon in the signal mode of the source. In practice, this means that the conversion efficiency (which depends on experimental parameters such as the nonlinearity and the pump power) must be limited so that the probability of multiple pair emission remains negligible. Let us note that other physical systems (e.g., biexcitonic decay in quantum dots [20]) are capable of true photon-pair emission. However, SPDC and SFWM remain highly flexible platforms for photon-pair emission, with entanglement characteristics which can be tailored according to the requirements of specific applications.

The dependence of the conversion efficiency on the fiber length L and on the pump bandwidths (σ_1 and σ_2) is not as simple to deduce from Eq. (19), compared to the pump power dependence, because these parameters are implicit in the joint spectral function [see Eq. (8)] which is given by a convolution-type integral. In general, as L increases, the joint spectral intensity $|f(\omega_s,\omega_i)|^2$ tends to exhibit a width in the space of generated frequencies which scales as L^{-1}. Equation (19) then tells us that the conversion efficiency tends to be linear in L. However, as we will see below, certain situations (such as nondegenerate pumps) can lead to a deviation from this linear behavior. Of course, a natural advantage of spontaneous four-wave mixing over spontaneous parametric down-conversion sources is that the interaction length can be increased easily, simply by increasing the fiber length (while, usually, nonlinear crystals tend to be limited in length to a scale of mm or cm).

While in general it is not possible to find a closed analytic expression for η, we will show in the next section that this becomes possible under certain approximations.

B. Pulsed pumps: Closed analytic expressions

In Ref. [6], we showed that it is possible to derive a closed analytic expression for the joint spectral amplitude [see Eq. (8)] if we resort to a linear approximation of the phase mismatch. Specifically, this approximation involves writing the phase mismatch [see Eq. (9)] as a first-order Taylor expansion in the frequency detunings $\omega_\mu - \omega_\mu^o$ (for $\mu = s,i$), where ω_μ^o represents the signal and idler frequencies for which perfect phase matching is obtained. Here, we exploit this approximation in order to obtain analytic expressions for the conversion efficiency.

We start by defining the function $h(\omega_s,\omega_i)$, which constitutes a factor in the integrand of the expression for the conversion efficiency [see Eq. (19)],

$$h(\omega_s,\omega_i) = \frac{\omega_s\omega_i k_s^{(1)}(\omega_s)k_i^{(1)}(\omega_i)}{n_s^2(\omega_s)n_i^2(\omega_i)}. \tag{20}$$

Next, we assume that $h(\omega_s,\omega_i)$ varies slowly over the spectral range of interest, so that we can consider it to be a constant when evaluating the integral in Eq. (19). We analyze first the general case in which the pumps are nondegenerate, i.e., where they can differ both in central frequency (ω_1^o and ω_2^o) and in bandwidth (σ_1 and σ_2). Following the treatment presented in Sec. 2 of Ref. [6] it is possible to find an analytic expression for the conversion efficiency η (NDP below refers to nondegenerate pumps), i.e.,

$$\eta^{\mathrm{NDP}} = \frac{2^5\hbar^2c^2n_1n_2\gamma^2N_1N_2}{(N_1+N_2)}\frac{\mathrm{erf}\left[(\sqrt{2}B)^{-1}\right]h\left(\omega_s^o,\omega_i^o\right)}{\left|k_1^{(1)}-k_2^{(1)}\right|\left|k_i^{(1)}-k_s^{(1)}\right|}, \tag{21}$$

where $k_\mu^{(1)} = k^{(1)}(\omega_\mu^o)$ (with $\mu = 1,2,s,i$), where $\mathrm{erf}(x)$ is the error function, and where we have defined the parameter B as [6]

$$B = \frac{\left(\sigma_1^2+\sigma_2^2\right)^{1/2}}{\sigma_1\sigma_2L\left[k_1^{(1)}-k_2^{(1)}\right]}. \tag{22}$$

Note that the only dependence of the conversion efficiency on the pump bandwidth and the fiber length is through the B parameter in the argument of the error function. The error function in Eq. (21) implies that η^{NDP} exhibits a saturation behavior when L or $\sigma_{1,2}$ vary, governed by the group-velocity mismatch between the two pumps. For example, we expect that as the fiber length is increased for fixed pump bandwidths, the conversion efficiency reaches a plateau at the point where the two pump pulses no longer overlap in time due to their different group velocities.

Let us now consider the degenerate-pump limit of Eq. (21). In this case, making $\sigma_1 = \sigma_2 \equiv \sigma$ and $P_1 = P_2 \equiv P$, in the limit $\omega_1^o \to \omega_2^o \equiv \omega^o$, Eq. (21) reduces to

$$\eta^{\mathrm{DP}} = \frac{2^4\hbar^2 c^2 n^2(\omega^o) L\sigma N\gamma^2}{\sqrt{\pi}\left|k_i^{(1)} - k_s^{(1)}\right|} h\left(\omega_s^o,\omega_i^o\right), \tag{23}$$

where DP denotes degenerate pumps. In the above equation it is possible to observe that the SFWM conversion efficiency increases linearly with fiber length and pump pulse bandwidth, at least within the frequency range in which the linear approximation for the phase mismatch is valid.

Note that in both the degenerate- and nondegenerate-pump cases, the emitted flux is inversely proportional to the group-velocity mismatch between signal and idler modes. As $k_s^{(1)}$ approaches $k_i^{(1)}$, the orientation of the phase-matching function in the generated frequencies space $\{\omega_s,\omega_i\}$ approaches that of the pump envelope function [6], with the implication that the emitted bandwidth increases, and consequently the generated flux also increases. In the case where $k_s^{(1)} = k_i^{(1)}$ (which would result from making the signal and idler frequencies degenerate), the linear approximation is no longer sufficient; second- and higher-order terms (not present within this approximation) prevent the resulting divergence in Eq. (21). From this analysis, it becomes clear that sources with a small signal-idler spectral separation tend to exhibit a considerably higher brightness than sources with a large signal-idler spectral separation.

C. Narrow-band-pump regimes

In this section, we focus our attention on SFWM photon-pair sources involving pumps in the monochromatic limit, i.e., for which $\sigma_{1,2} \to 0$. If the SFWM process takes place in a single transverse mode environment, such as a single-mode fiber, factorability is enforced on the transverse momentum degree of freedom, leaving frequency as the only continuous-variable degree of freedom where entanglement may reside. Let us note that SFWM sources based on narrow-band pumps permit the emission of photon pairs which are highly entangled in frequency [21]. Here we present an analysis of the conversion efficiency for this type of source.

In order to proceed with the calculation, we take the limit $\sigma_1 = \sigma_2 \equiv \sigma \to 0$ of the linear energy density $u_z(z,t)$ [see Eq. (12)] [21], obtaining the following time-independent expression

$$u_z(z) = \vartheta_{cw} \int dk_s \int dk_i \ell^3(\omega_s)\ell_D(\omega_s) \times \ell^2(\omega_i) k_s^{(1)} |F_{cw}(\omega_s,\omega_i)|^2, \tag{24}$$

in terms of the joint amplitude function $F_{cw}(\omega_s,\omega_i)$ and of the parameter ϑ_{cw}, given by

$$F_{cw}(\omega_s,\omega_i) = \delta(\omega_s + \omega_i - \omega_1 - \omega_2) \times \mathrm{sinc}\left[\frac{L}{2}\Delta k_{cw}(\omega_s,\omega_i)\right] e^{i\frac{L}{2}\Delta k_{cw}(\omega_s,\omega_i)}, \tag{25}$$

$$\vartheta_{cw} = \frac{2^3(2\pi)^2\epsilon_o^2 n_1 n_2 c^2}{\hbar^2\omega_1\omega_2} L^2\gamma^2 p_1 p_2,$$

where $\Delta k_{cw}(\omega_s,\omega_i)$ is the phase mismatch, which is now a function only of ω_s and ω_i, that is,

$$\Delta k_{cw}(\omega_s,\omega_i) = k\left[(\omega_s + \omega_i + \omega_1 - \omega_2)/2\right] + k[(\omega_s + \omega_i - \omega_1 + \omega_2)/2] - k(\omega_s) - k(\omega_i) - (\gamma_1 p_1 + \gamma_2 p_2). \tag{26}$$

In Eqs. (25) and (26), ω_ν represents the frequency and p_ν represents the average power for each of the two pump modes (with $\nu = 1,2$). Next, we define the spectral linear energy density $\mathscr{U}_z(k_s,z)$ corresponding to an optical mode with propagation constant k_s, such that $u_z(z) = \int dk_s \mathscr{U}_z(k_s,z)$. The signal-mode energy reaching a detector placed at position $z = z_D$ during a time interval Δt is then given by $\mathscr{U}(k_s) = \int_{z_D'}^{z_D} dz \mathscr{U}_z(k_s,z)$, where $z_D' = z_D - \Delta t/k_s^{(1)}$. Then, the signal-mode energy reaching the detector from all modes k_s is given by

$$U_s^{cw} = \int dk_s \mathscr{U}(k_s). \tag{27}$$

From Eq. (27), following a treatment similar to that used for the pulsed-pump case, it can be shown that the number of photons reaching the detector during time Δt is given by

$$N_{cw} = \frac{2^5 n_1 n_2 c^2 L^2\gamma^2 p_1 p_2 \Delta t}{\pi\omega_1\omega_2} \int d\omega h(\omega,\omega_1+\omega_2-\omega) \times \mathrm{sinc}^2[L\Delta k_{cw}'(\omega)/2], \tag{28}$$

where $\Delta k_{cw}'(\omega) = \Delta k_{cw}(\omega,\omega_1+\omega_2-\omega)$ and the function $h(\omega,\omega_1+\omega_2-\omega)$ is given according to Eq. (20).

The energy launched into the fiber corresponding to pump mode ν (with $\nu = 1,2$) during the time interval Δt is $U_\nu = p_\nu \Delta t$, so that the total photon number from two pumps in the time interval Δt can be obtained as

$$N_{p,cw} = \frac{p_1\omega_2 + p_2\omega_1}{\omega_1\omega_2}\frac{\Delta t}{\hbar}, \tag{29}$$

and therefore, the conversion efficiency $\eta_{cw} = N_s/N_{p,cw}$ in the process of SFWM with monochromatic pumps is given by

$$\eta_{cw} = \frac{2^5\hbar c^2 n_1 n_2}{\pi}\frac{L^2\gamma^2 p_1 p_2}{p_1\omega_2 + p_2\omega_1} \int d\omega h(\omega,\omega_1+\omega_2-\omega) \times \mathrm{sinc}^2[L\Delta k_{cw}'(\omega)/2]. \tag{30}$$

III. CONVERSION EFFICIENCY IN SPECIFIC SITUATIONS

In this section, we present the results of simulations of the expected conversion efficiency as a function of various experimental parameters: fiber length, pump power, and pump bandwidth. We also consider the dependence of the conversion efficiency on the type of spectral correlations between the signal and idler photons. Note that for these simulations, we have used the full two-photon state, i.e., we have not resorted to approximations. We compare these simulations with plots derived from the analytic expressions for the conversion efficiency presented in Sec. II B. We include in our analysis both the degenerate- and nondegenerate-pump configurations, as well as both the pulsed- and monochromatic-pump field

regimes. We assume that the SFWM process takes place in photonic crystal fibers (PCFs), which have been widely used for the experimental implementation of photon-pair sources [22–24]. PCFs are typically characterized by higher values of the nonlinearity coefficient γ, due to a large core-cladding dielectric contrast, as compared to typical telecommunications fibers. This leads to larger rates of emission, as is clear from Eqs. (19) and (30). Furthermore, PCFs permit the engineering of the fiber dispersion properties and therefore of the resulting photon-pair properties [6]. In the following three subsections, we specifically consider a PCF with a core radius of $r = 0.97$ μm and an air-filling fraction of $f = 0.91$; these values were chosen so that a zero dispersion point exists at $\lambda = 0.715$ μm. The fiber dispersion properties were calculated through the step-index model proposed in Ref. [25]. We assume a repetition rate for the pulsed-pump modes of $f_r = 80$ MHz, a fiber length of $L = 0.5$ m (except in Sec. III A where we study the fiber length dependence), an average pump power of $p = 300$ μW (except in Sec. III B, where we study the pump power dependence), and a pump bandwidth of $\sigma = 3.0$ THz (except in Sec. III C, where we study the pump bandwidth dependence).

For the degenerate-pump configuration, we assume that the pump pulses are centered at $\lambda_p = 0.708$ μm. This leads to a numerically calculated nonlinear coefficient, through Eq. (14), of $\gamma = 137$ km^{-1} W^{-1}. The pump peak power, with a value of 4.5 W, derived from $\sigma = 3$ THz and $p = 300$ μW, leads to generated signal and idler wave packets centered at 0.5759 and 0.9185 μm, respectively. For this source configuration, the signal and idler frequencies are nearly frequency-anticorrelated, with an orientation of the joint spectrum in $\{\omega_s,\omega_i\}$ space of $\theta_{si} = -40^\circ$ with respect to the ω_s axis [6].

For the nondegenerate-pump configuration, we assume that the two pump fields can be obtained as the fundamental and second-harmonic signal of the same laser system, thus facilitating the experimental implementation. As discussed in Ref. [6] this configuration permits the generation of signal and idler modes, which are sufficiently distant (in frequency) from the pumps, so that the signal and idler modes remain uncontaminated by photons produced by spontaneous Raman scattering. Specifically, we assume that the pump central wavelengths are $\lambda_1^0 = 0.521$ and $\lambda_2^0 = 1.042$ μm, which leads to a numerically calculated nonlinear coefficient for the SFWM interaction of $\gamma = 131$ km^{-1} W^{-1}; we note that this could be achieved with a Yb:KGW laser [26]. The values of the source parameters which we have assumed lead to signal and idler modes centered at $\lambda_s^o = 0.5826$ and $\lambda_s^o = 0.8600$ μm, respectively. Similar to the degenerate-pump case above, parameters were chosen so that this photon-pair source exhibits near-spectral anticorrelation, in this case with a joint spectrum oriented at -41° in $\{\omega_s,\omega_i\}$ space. It is worth mentioning that variations in the pump peak power (which can result from variations of the average power or bandwidth) can produce a shift of the signal and idler central generation frequencies due to the nonlinear term in Eq. (9) and could also produce variations of the types of signal-idler spectral correlations. However, we found that for the range of peak powers considered in the following simulations, these changes are negligible.

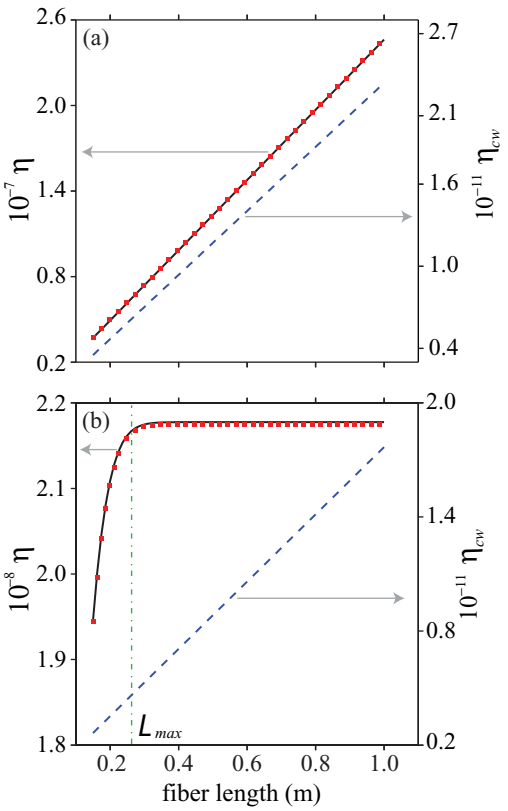

FIG. 1. (Color online) Conversion efficiency as a function of the fiber length for the pulsed and monochromatic pump regimes (denoted by η and η_{cw}, respectively), and for the following configurations: (a) degenerate pumps and (b) nondegenerate pumps. The red squares represent results obtained by numerical evaluation of Eq. (19). The solid-black line corresponds to results obtained from analytical expressions described in Sec. II B.

A. Fiber length dependence

Let us first consider the conversion efficiency for the photon-pair sources described above as a function of the fiber length. For the degenerate-pump configuration, the pump bandwidth which we have assumed ($\sigma = 3.0$ THz) corresponds to a width in wavelength of $\Delta\lambda = 0.94$ nm. The fiber length is varied between 0.15 and 1.0 m. The results obtained by numerical evaluation of Eq. (19) and those obtained from analytic expressions [Eq. (23)] are presented in Fig. 1(a). From this figure, it can be seen that numerical and analytical results are in good agreement over the full range of study, evidencing that the analytical expression derived in the linear approximation of the phase mismatch is in fact an excellent approximation. As predicted by Eq. (23), the conversion efficiency exhibits a linear dependence on fiber length. For the longest fiber considered ($L = 1.0$ m), approximately 5.3×10^8 photon pairs per second are emitted.

Likewise, considering the same fiber length range and average pump power as above, we evaluate the conversion efficiency η_{cw} as a function of the fiber length, in the monochromatic pump limit. Results obtained by numerical evaluation of Eq. (30) are represented in Fig. 1(a) by a dashed-blue line. It can be appreciated that the dependence of η_{cw} on L is, once again, linear. For the source parameters

which we have assumed and for the longest fiber length considered, approximately 5.0×10^4 photons/s are generated, which is much lower than the emission rate attainable in the pulsed-pump regime for the same fiber length. This reflects a general trend: the conversion efficiency is higher for pulsed pumps than for monochromatic pumps, because for SFWM (unlike for SPDC), the emission rate depends on the peak power (which increases with increasing pump bandwidths) rather than on the average pump power.

For the nondegenerate-pump configuration, we assume that the two pumps have the same bandwidth measured in frequency $\sigma_1 = \sigma_2 = 3$ THz, corresponding to $\Delta\lambda_1 = 0.51$ and $\Delta\lambda_2 = 2.03$ nm. It is also assumed that the pumps have the same average power, so that $P_1 = P_2$. Figure 1(b) shows the conversion efficiency as a function of fiber length, in the range 0.15–1.0 m. Clearly, there is an excellent agreement between numerical and analytical results calculated from Eqs. (19) and (21), respectively. In this figure, we can appreciate that if the fiber length exceeds a certain value, denoted by $L_{\max}$, the conversion efficiency reaches a plateau. This effect is related to the pulsed nature of the nondegenerate pump fields; the two fields experience different group velocities in the fiber. For a sufficiently long fiber, the pump pulses no longer overlap temporally, and therefore photon-pair generation ceases. $L_{\max}$ is defined as the value of L which makes the argument of the erf function in Eq. (21) equal to 2 (for which the erf function attains 99.5% of its maximum value), which leads to the following expression:

$$L_{\max} = \frac{2\sqrt{2}\sqrt{\sigma_1^2 + \sigma_2^2}}{\sigma_1\sigma_2\left|k^{(1)}(\omega_1^o) - k^{(1)}(\omega_2^o)\right|}. \tag{31}$$

This equation implies that for fixed pump bandwidths, the maximum interaction length between the pumps is determined by the difference of their reciprocal group velocities. Thus, pump fields with a considerable spectral separation will tend to exhibit a short maximum interaction length, which will be reflected in a low emission rate in comparison to that attainable in a degenerate-pump configuration, as is the case for the sources assumed for Fig. 1(a). In the particular case of Fig. 1(b), the maximum interaction length is $L_{\max} = 0.263$ m and 5.12×10^7 photon pairs per second are generated for a fiber of length $L = L_{\max}$. Of course, if the temporal duration of the pump pulses is increased, this will tend to increase the maximum interaction length, since the mode-1 and mode-2 pulses will remain temporally overlapped over a longer length of fiber. Results obtained for the monochromatic-pump regime are also shown in Fig. 1(b). In this case we assumed the same pump power and fiber lengths as above. It can be appreciated that the conversion efficiency increases linearly with fiber length over the full range of fiber length values. Indeed, for nondegenerate monochromatic pumps, there is no maximum interaction length.

From these results, it is evident that pulsed-pump regimes (both in the degenerate- and nondegenerate-pump configurations) lead to much higher conversion efficiencies than monochromatic-pump regimes. This will also be clear from the discussion in Sec. III C, where we analyze the conversion efficiency as a function of pump bandwidth. While nondegenerate pumps lead to a lower conversion efficiency compared to degenerate pumps (for given pump bandwidths), in this case the effect is much less drastic than for pulsed versus monochromatic pumps. Nondegenerate-pump schemes offer some advantages over degenerate-pump schemes, despite the resulting lower emission rates, especially in relation to the ability to generate signal and idler photons away from the Raman gain bandwidth of fused silica [21].

B. Pump power dependence

We now turn our attention to the pump power dependence, while maintaining the pump bandwidths fixed, of the conversion efficiency. In order to compare sources with pulsed and monochromatic pumps, we compute the conversion efficiency as a function of the *average* pump power together with, for the pulsed-pump case, a certain value assumed for the repetition rate which characterizes the pump-pulse train. We consider the sources described above and vary the average pump power between 0.05 and 1.0 mW. Under these conditions, for a repetition rate of $f_r = 80$ MHz, the pump peak power varies within the range 0.75–15 W, without an appreciable resulting variation of the spectral properties of the two-photon state. Plots derived from our expressions [Eqs. (19) and (23)] are presented in Fig. 2(a),

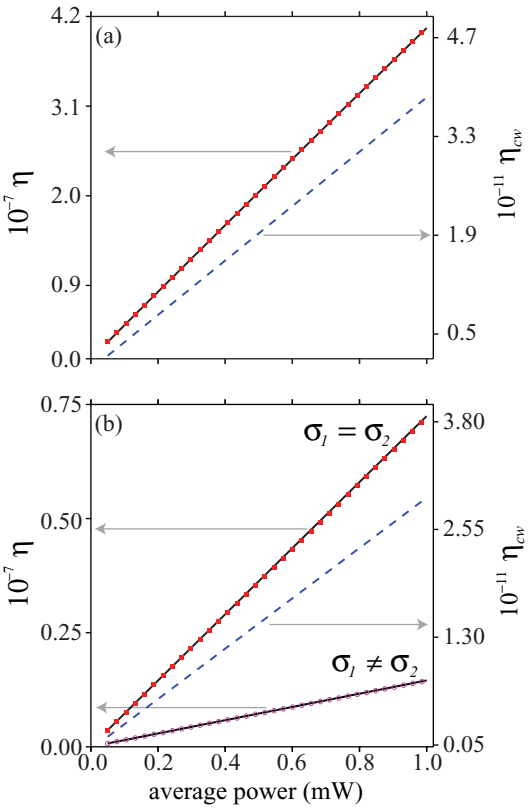

FIG. 2. (Color online) Conversion efficiency as a function of average pump power, for pulsed- and monochromatic-pump regimes (denoted by η and η_{cw}, respectively), and for the following configurations: (a) degenerate pumps and (b) nondegenerate pumps. The red squares and magenta circles are results obtained by numerical evaluation of Eq. (19), while the solid-black line corresponds to results obtained from analytical expressions described in Sec. II B.

from which it is clear that the conversion efficiency η is linear with pump power. Note that this linear dependence becomes quadratic, if the emitted flux N_s, rather than the conversion efficiency, were to be plotted versus average pump power. This is a different behavior from that observed for the generation of photons pairs through spontaneous parametric down-conversion (SPDC) in second-order nonlinear materials, for which the conversion efficiency versus average power is constant, while the emitted flux versus pump power is linear. This is related to the fact that two pumps, rather than one, are required for SFWM. In fact, this represents one of the essential advantages of SFWM over SPDC photon-pair sources: while both processes are spontaneous, in some respects such as pump power dependence, SFWM behaves as a stimulated process exhibiting the same pump power dependence as second-order nonlinear processes such as second-harmonic generation. At the highest average pump power considered, Eq. (19) predicts the generation of 2.89×10^9 photon pairs per second. For the corresponding monochromatic-pump case [see dashed-blue line in Fig. 2(a)], the number of photon pairs generated for the highest pump power considered becomes 2.75×10^5 per second.

For the case of pulsed, nondegenerate pumps we can analyze two distinct configurations. On the one hand, the pumps can be nondegenerate in frequency, with the same bandwidth so that $\sigma_1 = \sigma_2 \equiv \sigma$, which implies that the corresponding peak powers are equal, i.e., $P_1 = P_2$, if we assume the same repetition rate for both pump modes. The numerical and analytical results obtained from Eqs. (19) and (21) are shown in Fig. 2(b) (red squares and solid-black line, respectively). As shown, at the highest average power considered, around 5.7×10^8 photons per second are emitted. On the other hand, the bandwidth of the two pump modes can be different. In this case, for the same average power and repetition rate, the peak powers are no longer equal, i.e., $P_1 \neq P_2$. In particular, we consider the limiting case where the pump bandwidths are highly unequal, i.e., $\sigma_1 \ll \sigma_2$ (or $\sigma_2 \ll \sigma_1$). In Fig. 2(b) we present results for $\sigma_1 = 0.1$ and $\sigma_2 = 3.0$ THz, where we assume the same fiber length as above (numerical, magenta circles; analytical, solid-black line). It can be appreciated that these unbalanced pump bandwidths lead to an important reduction in the conversion efficiency η (while maintaining the average pump power constant). The highest average pump power considered results in 1.1×10^8 photon pairs emitted per second. This behavior can be understood from Eqs. (21) and (22), from which we can show that the condition $\sigma_1 \ll \sigma_2$ implies that $\mathrm{erf}[1/\sqrt{2}B] \ll 1$. As in previous cases, we can observe in Fig. 2 that analytical results are in excellent agreement with numerical ones.

For comparison, the conversion efficiency derived from Eq. (30) in the monochromatic-pump regime is also shown in Fig. 2(b) (dashed-blue line). It can be appreciated that the conversion efficiency in this configuration is several orders of magnitude lower than for the pulsed-pump case. Assuming $p_1 = p_2$, the emission rate at the highest pump power considered is 2.3×10^5 photon pairs per second. This is to be compared with a corresponding emission rate of 5.7×10^8 photon pairs per second in the (nondegenerate) pulsed-pump regime, assuming the same average pump power and a repetition rate of 80 MHz, when pumps have the same bandwidth. Thus, as has been discussed before, the conversion efficiency in the monochromatic-pump regime tends to be significantly lower than for the pulsed-pump regime.

C. Pump bandwidth dependence

In this section we turn our attention to the pump-bandwidth dependence of the conversion efficiency (while maintaining the energy per pulse, or alternatively the average power and the repetition rate, in each of the two pump modes constant). We consider the same source parameters as above. Of course, as σ varies, the pulse temporal duration varies, and consequently the peak power varies too. We consider first the degenerate-pump configuration. We evaluate the conversion efficiency from Eqs. (19) and (23) for a pump bandwidth σ range 0.05–4.0 THz (which corresponds to a Fourier-transform-limited temporal duration range 0.59–47.07 ps). Numerical results [obtained from Eq. (19)] as well as analytical results [from Eq. (23)] are shown in Fig. 3(a), exhibiting good agreement and, for small σ, a linear dependence of the conversion efficiency on σ. Note that for large values of σ, there can be a deviation from the linear trend apparent in Fig. 3(a). Indeed, large values of σ translate into greater spectral width of the signal and idler wave packets, with the effect that the linear approximation of the phase mismatch [upon which Eq. (23) is based] no

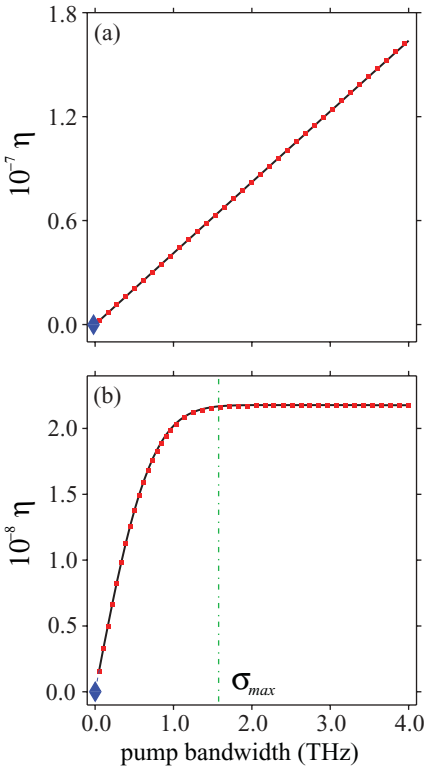

FIG. 3. (Color online) Conversion efficiency as a function of pump bandwidth, for pulsed and monochromatic pump regimes (denoted by η and η_{cw}, respectively), and for the following configurations: (a) degenerate pumps and (b) nondegenerate pumps. The red squares are results obtained by numerical evaluation of Eq. (19), while the solid-black line corresponds to results obtained from analytical expressions described in Sec. II B. The blue diamonds represent the conversion efficiency in the limit of monochromatic pumps.

longer suffices. In the monochromatic limit, evaluation of the conversion efficiency through Eq. (30) predicts a value of $\eta_{cw} = 1.156 \times 10^{-11}$. The blue diamond in Fig. 3(a) indicates the conversion efficiency in this limit; it is graphically clear that the conversion efficiency values for $\sigma \neq 0$ [calculated from Eq. (19)] approach the monochromatic-pump limit [calculated from Eq. (30)].

We now consider the nondegenerate-pump case. We vary σ in the range 0.05–4.0 THz and assume the same fiber length, average pump power, and repetition rate as for the degenerate-pump case. Figure 3(b) shows numerical results indicated by red squares superimposed with analytical results [from Eq. (21)] indicated by the solid-black line. Let us note that in this case, the flux dependence versus σ is linear for small σ, and exhibits a saturation effect around a specific value of σ to be referred to as $\sigma_{\max}$. In order to understand this saturation effect, we note that while the pump pulses remain temporally overlapped (as in the degenerate case discussed above), the conversion rate has a linear dependence on σ. However, for nondegenerate pumps, the two pump modes propagate at different group velocities, and the resulting maximum interaction length is given as in Eq. (31), which for $\sigma_1 = \sigma_2 \equiv \sigma$ scales as σ^{-1}. This interaction length which decreases with σ offsets the conversion efficiency per unit fiber length which scales as σ, leading to the saturation effect. The bandwidth at which saturation occurs, $\sigma_{\max}$, is defined as the value of σ which makes the argument of the erf function in Eq. (21) equal to 2 (for which the erf function attains 99.5% of its maximum value), which leads to the following expression

$$\sigma_{\max} = \frac{4}{L\left|k^{(1)}\left(\omega_1^o\right) - k^{(1)}\left(\omega_2^o\right)\right|}. \tag{32}$$

In the specific case which we have modeled, $\sigma_{\max} = 1.58$ THz, which is indicated by a vertical dot-dashed line in Fig. 3(b). As shown in the figure, the largest considered pump bandwidth leads to a conversion efficiency of $\eta = 2.18 \times 10^{-8}$, which corresponds to 5.13×10^7 photon pairs emitted per second. The corresponding conversion efficiency obtained when pumps are in the monochromatic limit is $\eta_{cw} = 8.7 \times 10^{-12}$ and is indicated in the figure by the blue diamond. It is graphically clear that the conversion efficiency values for $\sigma \neq 0$ [calculated from Eq. (19)] approach the monochromatic-pump limit [calculated from Eq. (30)]. We note that if the spectral separation between the two pump modes is not too great, temporal broadening of the pump pulses due to second-order and higher-order dispersion effects lead to some overlap between the pulses in the two modes even for large values of σ. This implies that under these circumstances, the conversion efficiency does not reach a strict plateau for $\sigma > \sigma_{\max}$.

Let us note that the behavior of SFWM sources in terms of the pump-bandwidth dependence of the conversion efficiency is different from that observed for photon-pair sources based on SPDC. In the case of SPDC sources, the corresponding dependence is constant within the phase-matching bandwidth of the nonlinear crystal. As in the discussion related to pump-power dependence, SFWM sources behave, in terms of the observed linear dependence of the conversion efficiency on pump bandwidth, as a second-order nonlinear stimulated nonlinear process, such as second-harmonic generation, would. This has an important consequence: because the spontaneous Raman scattering flux, which tends to degrade the quality of the source, exhibits a constant dependence on σ [27,28], by increasing σ (which corresponds to shortening the temporal duration of pump pulses), we can diminish the relative weight of spontaneous Raman scattering as a fraction of the total emitted light.

D. Dependence on type and degree of spectral correlations

We have shown in Refs. [6,21,29] that it is possible to engineer the spectral entanglement properties of photon pairs generated by SFWM sources. Recent experimental results [24,30,31] confirm the ability of engineered sources to generate, in particular, factorable photon pairs. In this context, it is natural to ask how the conversion efficiency depends on the type of spectral correlations observed, a question which represents the focus of this section.

In Ref. [6] we showed that the spectral entanglement properties of the generated photon pairs can be controlled by the pump frequency. For a fiber with two zero-dispersion points within the spectral region of interest, which can be the case of a photonic crystal fiber (PCF), the generated signal and idler frequencies form a loop in the space of generated frequencies versus pump frequency. Each point around the loop corresponds to a specific angle of orientation (covering all possible values between 0 and 2π radians) of the phase-matching function in the space of generated frequencies $\{\omega_s, \omega_i\}$. We will illustrate our discussion considering a degenerate-pump SFWM source based on a PCF with a core radius of $r = 0.5$ μm and an air-filling fraction of $f = 0.6$, which exhibits zero dispersion points at 0.6592 and 0.8595 μm (note that this is a different fiber geometry from that assumed for the last three subsections). For a pump wavelength $\lambda_p = 0.75$ μm, we obtained a value of the nonlinearity coefficient of $\gamma = 337\,\mathrm{km}^{-1}\,\mathrm{W}^{-1}$, through numerical integration of Eq. (14). We assume the following choice of parameters: average pump power of $p = 300$ μW, pump bandwidth of $\sigma = 5$ THz, and fiber length of $L = 1$ m. Let us note that we have assumed a sufficiently large pump bandwidth, so that the photon-pair correlations are determined by the phase-matching function rather than by the pump pulse bandwidth.

Figure 4(a) shows a plot of the $\Delta k = 0$ contour (the solid-black curve) in the $\{\omega_p, \Delta_{s,i}\}$ space, where the generated frequencies are expressed as detunings from the pump frequency $\Delta_{s,i} = \omega_{s,i} - \omega_p$. Likewise, in this figure the phase-matching orientation angle (θ_{si}), in the $\{\omega_s, \omega_i\}$ space, is represented by the colored background, where it can be seen that this ranges from $\theta_{si} = -90^\circ$ to $\theta_{si} = +90^\circ$, indicated in blue and red, respectively. Note that phase matching occurs within a range of approximately 200 nm. Here, we will concentrate on the "outer-branch" solutions (as opposed to the "inner-branch" solutions which flank the pump frequency, represented by $\Delta_{s,i} = 0$, at a much smaller spectral separation). The outer branch is sufficiently removed from the pump that contamination by photons generated by spontaneous Raman scattering may be avoided.

We compute the conversion efficiency as a function of the pump frequency, covering the following wavelength range:

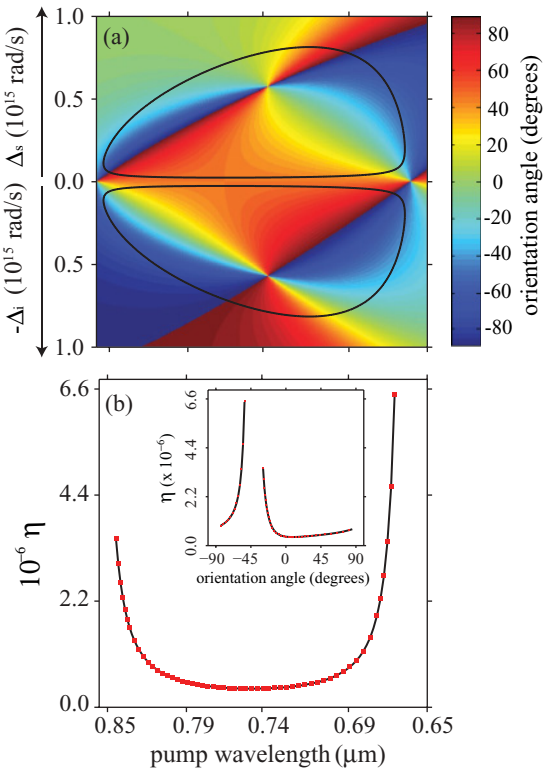

FIG. 4. (Color online) (a) Solid-black curve: phase-matching ($\Delta k = 0$) contour for SFWM in the degenerate-pump case. Colored background: phase-matching orientation angle. Note that the pump frequency axis has been labeled with the corresponding wavelength values. (b) Conversion efficiency as a function of the pump frequency, varied within the range for which perfect phase-matching occurs. The inset corresponds to the conversion efficiency η, expressed as a function of the orientation angle.

0.666–0.843 μm. Fig. 4(b) shows the conversion efficiency obtained numerically from Eq. (19) (red squares) and the conversion efficiency obtained analytically from Eq. (23) (solid-black line). Because in general to each pump frequency corresponds a given phase-matching orientation angle value, these results can be also plotted as a function of the orientation angle, as shown in the inset of Fig. 4(b). From these results, it is clear that anticorrelated two-photon states, characterized by $\theta_{si} = -45^\circ$, lead to a larger conversion efficiency as compared to other orientations in $\{\omega_s, \omega_i\}$ space. The physical reason for this greater conversion efficiency is that for $\theta_{si} = -45^\circ$, the phase-matching function overlaps the pump envelope function over a wider spectral range, leading to a greater generation bandwidth which tends to enhance the value of the integral in Eq. (19). This behavior is also consistent with Eqs. (21) and (23), where if $k_s^{(1)} = k_i^{(1)}$, which corresponds to $\theta_{si} = -45^\circ$, the conversion efficiency diverges (within the linear approximation of the phase mismatch) and increases markedly if higher-order terms are taken into account. Note that the agreement between numerical and analytical results in Fig. 4(b) is excellent. While we concentrated our discussion in this section on the degenerate-pump case, very similar conclusions apply for the nondegenerate case.

IV. CONCLUSIONS

In this paper we have focused on the conversion efficiency of pump photons into signal and idler photon pairs in the process of copolarized, spontaneous four-wave mixing in single-mode optical fibers. We have derived expressions for the conversion efficiency, defined as the signal-mode, single-photon flux divided by the pump flux, as a function of all relevant experimental parameters. Our analysis includes on the one hand both the monochromatic- and the pulsed-pump regimes, and on the other hand both the degenerate- and nondegenerate-pump configurations. These expressions are written in terms of two-dimensional integrals, which for the case of pulsed pumps we take to closed analytic form under certain approximations. We present plots of the conversion efficiency as a function of experimental parameters, including fiber length, pump power, and pump bandwidth, computed through numerical integration of our conversion efficiency expressions. We verify that the corresponding conversion efficiency values computed from our expressions in closed analytic form, for pulsed pumps, are in good agreement. We find that the behavior of the conversion efficiency with respect to pump power and pump bandwidth is strikingly different from that observed for spontaneous parametric down-conversion. In particular, the linear dependence of the conversion efficiency on pump power (compared to the constant dependence observed for SPDC) and the linear dependence of the conversion efficiency on pump bandwidth in the case of degenerate pumps (compared to the constant dependence observed for SPDC) favor the design of bright photon-pair sources. We hope that this work will be useful in the design of fiber-based, photon-pair sources, for the next generation of quantum-information processing experiments.

ACKNOWLEDGMENTS

This work was supported in part by CONACYT, Mexico, by DGAPA, UNAM, and by FONCICYT project 94142.

[1] A. Zeilinger, Rev. Mod. Phys. **71**, S288 (1999).
[2] P. Kok, W. J. Munro, K. Nemoto, T. C. Ralph, J. P. Dowling, and G. J. Milburn, Rev. Mod. Phys. **79**, 135 (2007).
[3] D. C. Burnham and D. L. Weinberg, Phys. Rev. Lett. **25**, 84 (1970).
[4] J. E. Sharping, M. Fiorentino, A. Coker, P. Kumar, and R. S. Windeler, Opt. Lett. **26**, 1048 (2001).
[5] K. F. Lee, J. Chen, Ch. Liang, X. Li, P. L. Voss, and P. Kumar, Opt. Lett. **31**, 1905 (2006).
[6] K. Garay-Palmett, H. J. McGuinness, O. Cohen, J. S. Lundeen, R. Rangel-Rojo, M. G. Raymer, C. J. McKinstrie, S. Radic, A. B. U'Ren, and I. A. Walmsley, Opt. Express **15**, 14870 (2007).
[7] M. A. Arbore, M. M. Fejer, M. E. Fermann, A. Hariharan, A. Galvanauskas, and D. Harter, Opt. Lett. **22**, 13 (1997).

[8] R. Krischek, W. Wieczorek, A. Ozawa, N. Kiesel, P. Michelberger, T. Udem, and H. Weinfurter, Nat. Photon. **4**, 170 (2010).
[9] J. Fulconis, O. Alibart, W. J. Wadsworth, and J. G. Rarity, New J. Phys. **9**, 276 (2007).
[10] J. Chen, X. Li, and P. Kumar, Phys. Rev. A **72**, 033801 (2005).
[11] O. Alibart, J. Fulconis, G. K. L. Wong, S. G. Murdoch, W. J. Wadsworth, and J. G. Rarity, New J. Phys. **8**, 67 (2006).
[12] E. Brainis, Phys. Rev. A **79**, 023840 (2009).
[13] L. Mandel and E. Wolf, *Optical Coherence and Quantum Optics* (Cambridge University, New York, 1995).
[14] M. H. Rubin, D. N. Klyshko, Y. H. Shih, and A. V. Sergienko, Phys. Rev. A **50**, 5122 (1994).
[15] G. P. Agrawal, *Nonlinear Fiber Optics*, 4th ed. (Elsevier, New York, 2007).
[16] The nonlinear contribution to the phase mismatch can be shown to be given by $(\gamma_1 + 2\gamma_{21} - 2\gamma_{s1} - 2\gamma_{i1})P_1 + (\gamma_2 + 2\gamma_{12} - 2\gamma_{s2} - 2\gamma_{i2})P_2$, where γ_1 and γ_2 result from self-phase modulation and the remaining γ terms correspond to various cross-phase modulation contributions. It may be shown that for the sources considered in this paper, the following represent valid approximations: $\gamma_1 \approx \gamma_{21} \approx \gamma_{s1} \approx \gamma_{i1}$ and $\gamma_2 \approx \gamma_{12} \approx \gamma_{s2} \approx \gamma_{i2}$. Under these approximations, we arrive at Eq. (9).
[17] Note that while γ_1 and γ_2 are related to cross- and self-phase modulation effects, γ governs the SFWM interaction.
[18] L. Tong, J. Lou, and E. Mazur, Opt. Express **12**, 1025 (2004).
[19] M. A. Foster, K. D. Moll, and A. L. Gaeta, Opt. Express **12**, 2880 (2004).
[20] O. Benson, C. Santori, M. Pelton, and Y. Yamamoto, Phys. Rev. Lett. **84**, 2513 (2000).
[21] K. Garay-Palmett, A. B. U'Ren, R. Rangel-Rojo, R. Evans, and S. Camacho-Lopez, Phys. Rev. A **78**, 043827 (2008).
[22] J. Rarity, J. Fulconis, J. Duligall, W. Wadsworth, and P. S. J. Russell, Opt. Express **13**, 534 (2005).
[23] J. Fan and A. Migdall, Opt. Express **13**, 5777 (2005).
[24] O. Cohen, J. S. Lundeen, B. J. Smith, G. Puentes, P. J. Mosley, and I. A. Walmsley, Phys. Rev. Lett. **102**, 123603 (2009).
[25] G. K. L. Wong, A. Y. H. Chen, S. W. Ha, R. J. Kruhlak, S. G. Murdoch, R. Leonhardt, J. D. Harvey, and N. Y. Joly, Opt. Express **13**, 8662 (2005).
[26] A. Major, V. Barzda, P. A. E. Piunno, S. Musikhin, and U. J. Krull, Opt. Express **14**, 5285 (2006).
[27] Q. Lin, F. Yaman, and G. P. Agrawal, Phys. Rev. A **75**, 023803 (2007).
[28] M. G. Raymer and J. Mostowski, Phys. Rev. A **24**, 1980 (1981).
[29] K. Garay-Palmett, R. Rangel-Rojo, and A. B. U'Ren, J. Mod. Opt. **55**, 3121 (2008).
[30] M. Halder, J. Fulconis, B. Cemlyn, A. Clark, C. Xiong, W. J. Wadsworth, and J. G. Rarity, Opt. Express **17**, 4670 (2009).
[31] C. Söller, B. Brecht, P. J. Mosley, L. Y. Zang, A. Podlipensky, N. Y. Joly, P. S. J. Russell, and C. Silberhorn, Phys. Rev. A **81**, 031801(R) (2010).